Optics Letters

Multi-channel mode converter based on a modal interferometer in a two-mode fiber

Guolu Yin,[1,2,*] Changle Wang,[2] Yunhe Zhao,[2] Biqiang Jiang,[2] Tao Zhu,[1] Yiping Wang,[3] and Lin Zhang[2]

[1]Key Laboratory of Optoelectronic Technology & Systems (Ministry of Education), Chongqing University, Chongqing 400044, China
[2]Institute of Photonic and Technologies, Aston University, Birmingham B4 7ET, UK
[3]Key Laboratory of Optoelectronic Devices and Systems of Ministry of Education and Guangdong Province, College of Optoelectronic Engineering, Shenzhen University, Shenzhen 518060, China
*Corresponding author: glyin@cqu.edu.cn

Received 26 July 2017; revised 25 August 2017; accepted 27 August 2017; posted 29 August 2017 (Doc. ID 301850); published 19 September 2017

In this Letter, we propose a multi-channel mode converter with the concept of a modal interferometer in a two-mode fiber (TMF). Two lateral stress points in a TMF function as in-line fiber mode couplers to construct the modal interferometer, and both transmission spectra and near-field patterns confirm that the LP_{01} mode is successfully converted into an LP_{11} mode at the multiple channels. The measured mode conversion efficiency almost completely follows the theoretical tendency. Finally, the mode conversion is realized at 20 channels in the C + L wavelength band with conversion efficiency up to 99.5% and insertion loss as low as 0.6 dB. Furthermore, the channel spacing can be freely tailored by adjusting the distance between two stress points.

OCIS codes: (060.2340) Fiber optics components; (060.2330) Fiber optics communications; (060.4230) Multiplexing; (260.3160) Interference.

https://doi.org/10.1364/OL.42.003757

The standard single-mode fiber (SMF) optical network is speedily approaching the theoretical capacity limitation in the last decade [1,2]. A new key technological breakthrough is imminently required to substantially increase the per-fiber capacity. Mode-division multiplexing (MDM) in a few-mode fiber (FMF) is a promising approach to exploit the spatial domain for overcoming current limitations of the transmission capacity in a SMF [3,4]. In the MDM system, the mode converter is required to convert the fundamental mode in standard SMFs into higher-order modes in FMFs. Various schemes for mode multiplexing have been reported. The most well-known and widely used technique is based on spatial light modulators [5] or phase plates [6], but it is complicated and difficult for bulk devices to align the optical path, resulting in a large coupling loss. For instance, the mode converter based on a liquid crystal on a silicon spatial modulator has a conversion loss of approximately 9 dB [7]. Photonic integrated circuits also were proposed as mode converters, but the FMF needs angular alignment to the integrated chip; even so, the coupling loss between the fiber and integrated chip is as high as 6–7 dB [8]. A low-loss and low-crosstalk mode converter based on a two-core directional coupler has been demonstrated to realize two-mode coupling [9]; then a three-core tapered mode coupler was theoretically analyzed [10] and experimentally demonstrated [11] to excite both LP_{11a} and LP_{11b} modes separately. A photonic lantern was reported to convert multiple beams into the super-mode in the FMF [12], while multiple-input and multiple-output processing is required to compensate for the signal crosstalk. Another kind of in-fiber mode converter is based on fiber gratings fabricated by an ultraviolet laser [13], a CO_2 laser [14,15], an acoustic method [16], and a mechanical method [17–19]. However, grating-based mode converters only work at a single wavelength and have limited optical bandwidth and, hence, they are not practical to be applied in wavelength and MDM communication systems.

In this Letter, we propose a multi-channel mode converter in a two-mode fiber (TMF). A modal interferometer was designed to convert the LP_{01} to the LP_{11} mode in the TMF. The multiple phase matching points in the modal interferometer ensure the proposed mode converter can work at multi-channel wavelengths. We investigated both the transmission spectra and the near-field mode patterns to confirm the multi-channel mode conversion. Such mode converters would find potential applications in wavelength and MDM systems.

Figure 1 illustrates the schematic of our proposed multi-channel mode converters in the TMF. The TMF is employed to support a fundamental mode LP_{01} and the second-order mode LP_{11}. A standard SMF is spliced to a TMF for exciting the LP_{01} mode purely. To mechanically induce mode coupling from the LP_{01} to LP_{11} modes, two bare metal plates are employed to introduce stress to the TMF to form the multi-channel mode converter. At the first stress point, the input light is partly coupled into LP_{11} mode, and the rest is still guided in the LP_{01} mode. After the first stress point, both modes propagate in the TMF. Due to the propagation constant mismatch, the phase difference is generated between the LP_{01} and LP_{11} modes. When the two modes arrive at the second stress

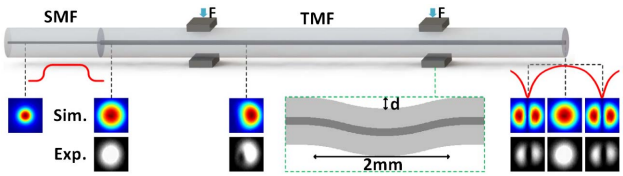

Fig. 1. Schematic of the multi-channel mode converter in a TMF. SMF, single-mode fiber; TMF, two-mode fiber; F, force. Inset: S-bend at the stress point; d: core-offset of the S-bend.

point, part of LP_{11} mode is coupled back to the LP_{01} mode, while part of the LP_{01} mode is coupled to LP_{11} mode again. Consequently, the two stress points function as two in-line fiber mode couplers to construct a modal interferometer for achieving multi-channel mode converter.

In the in-line fiber modal interferometer, it is hard to measure the transmission spectra in LP_{11} mode directly; we measured the interference spectra in the LP_{01} mode by splicing a leading out SMF to the TMF, and the spectral profile of LP_{11} mode can be interpreted by the inverse of the spectral profile of the LP_{01} mode. The interference spectral profile of the LP_{01} mode is the cosine function of phase difference between the LP_{01} and LP_{11} modes. Assuming the input LP_{01} mode has normalized intensity, the output spectrum of the LP_{01} mode can be expressed as follows:

$$I_{\text{out}} = \alpha_{01}^2 + \alpha_{11}^2 - 2\alpha_{01}\alpha_{11}\cos\phi, \tag{1}$$

with a phase difference

$$\phi = 2\pi\Delta n_{\text{eff}} L/\lambda, \tag{2}$$

where α_{01} and α_{11} are the split ratios of the LP_{01} and LP_{11} modes at the stress point, respectively, Δn_{eff} is the effective refractive index difference between the two modes, L is the length of the mode converter, which is defined as the distance between two stress points. When the phase difference is an odd multiple of π, constructive interference occurs, and the light is still confined in the LP_{01} mode, showing peaks in the spectrum. When the phase difference is an even multiple of π, destructive interference occurs, and the light is converted from an LP_{01} into an LP_{11} mode, showing dips in the spectrum. Therefore, multiple-mode conversion is expected at the multiple dips, and the kth mode conversion from LP_{01} to LP_{11} mode occurs at the wavelength

$$\lambda_{01-11}^{k} = \frac{\Delta n_{\text{eff}} L}{k}, \tag{3}$$

where k is an integer. At these mode conversion wavelengths, the mode conversion efficiency is expressed as

$$\eta = 1 - (\alpha_{01} - \alpha_{11})^2. \tag{4}$$

According to Eq. (4), the LP_{01} mode can be fully converted into an LP_{11} mode if both modes have the same split ratio at the stress point. Since the proposed mode converter has multiple working channels, the channel spacing is expressed as

$$\Delta\lambda = \frac{\lambda^2}{\Delta m L}, \tag{5}$$

with the group differential modal index

$$\Delta m = \Delta n_{\text{eff}} - \lambda\frac{\partial\Delta n_{\text{eff}}}{\partial\lambda}. \tag{6}$$

From Eq. (5), it is found that the channel spacing is mainly determined by the fiber dispersion property and the device length. For a given TMF, the channel spacing can be easily tailored by changing the distance between the two stress points.

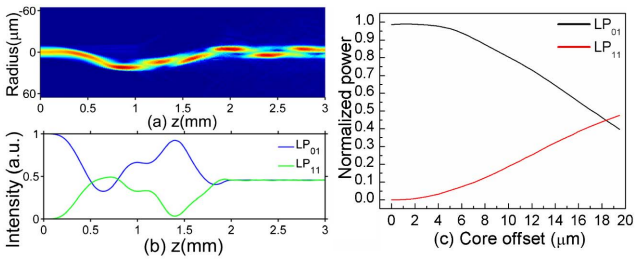

Fig. 2. Theoretical analyses in the S-bend section. (a) Optical propagation and (b) mode coupling in a 2 mm S-bend section and a 1 mm straight fiber; (c) normalized power in the LP_{01} and LP_{11} modes as a function of the core-offset at the S-bend section.

At the stress point, the TMF was laterally stressed from above, and physical deformation was inevitably produced. Such deformation can be simply modeled as an S-bend arc [20], as shown in Fig. 1. The deformed fiber length is around 2 mm, and the deformed strength is quantitatively evaluated by the core offset, i.e., d. We employed the beam propagation method to simulate the light transmission in a 2 mm S-bend section and a 1 mm straight fiber with a pure LP_{01} input. As shown in Fig. 2(a), except for a small amount of light excited into the cladding, the overwhelming majority of the light still propagates in the core region. Due to the lateral stress, the light can be easily coupled between the symmetrical LP_{01} mode and the asymmetrical LP_{11} mode. When both modes exist in the fiber, the spatial interference between the LP_{01} and LP_{11} modes leads to asymmetric field patterns. The different propagation constants of both modes cause a mode beating along the propagation direction. The beating results in a zigzag-like optical path.

The S-bend section functions as an in-line fiber coupler to split the input mode into both LP_{01} and LP_{11} modes, and the corresponding normalized light intensities depend on the deformed core-offset. Taking the LP_{01} mode as the input mode, Fig. 2(c) illustrates the intensity evolution in both modes when the deformed core-offset is set in the range from 0 to 19.5 μm. With the increase in the deformed core-offset, the light intensity in the LP_{01} mode gradually decreases, and the diminished light is coupled into the LP_{11} mode; hence, the LP_{11} mode component gradually increases. At the core-offset of around 18.5 μm, both modes hold almost the same light intensity. Figure 2(b) illustrates the mode coupling from the LP_{01} to the LP_{11} mode in a 2 mm S-bend section with a core-offset of 18.5 μm. It is found that, after the S-bend section, the LP_{01} and LP_{11} modes account for 44% and 45% light intensity, respectively. When the input mode was replaced by the LP_{11} mode, the mode coupling from the LP_{11} to LP_{01} was also realized in the S-bend section, and similar splitting ratio was observed. In other words, the S-bend section with a core-offset of 18.5 μm functions as a 50:50 in-line fiber mode coupler. If such two S-mode couplers were cascaded to construct a modal interferometer, a high contrast would be predicted in the interference fringe pattern. Furthermore, according to Eq. (4), a high-mode conversion efficiency is expected at the multiple spectral dips for converting the LP_{01}–LP_{11} modes.

In our experiments, we employed the two-mode step-index fiber from OFS to support the LP_{01} and LP_{11} modes. The TMF

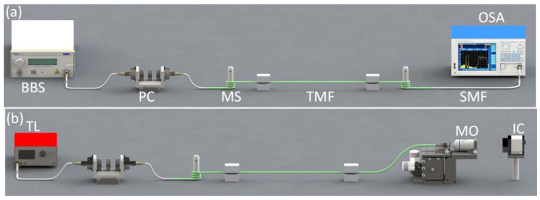

Fig. 3. Schematic of the experimental setups for measuring (a) the transmission spectrum and (b) the near-mode field profiles of the proposed multiple-channel mode converter. BBS, broadband source; TL, tunable laser; PC, polarization controller; MS, mode striper; TMF, two-mode fiber; SMF, single-mode fiber; OSA, optical spectrum analyzer; MO, microscope objective; IC, infrared camera.

has a core diameter of 19.5 μm and a cladding diameter of 125 μm, a cladding index of 1.444, and a core index of 1.449. Figure 3(a) illustrates the experimental setup for measuring the spectral response of our proposed multiple-mode converters. A broadband source was launched into the SMF, and then spliced to the TMF with low insertion loss. The LP_{01} mode in the TMF was excited with high-mode purity by the direct-splicing method. Moreover, the TMF was tightly wrapped around a 12 mm diameter still roll, working as a mode stripper to further suppress the unintended LP_{11} mode and to ensure a pure LP_{01} launching before the first stress point. After the second stress point, another mode stripper was also used to attenuate the generated LP_{11} mode, making sure only the LP_{01} mode was coupled back to the leading out-SMF for measuring the transmission spectra.

We optimized the mode conversion efficiency by changing the weights at both stress points. Figure 4(a) illustrates the several typical transmission spectra of the mode converter with $L = 75$ cm when the applied force was increased to 50, 100, 250, 200, and 250 g. At the peaks, the light is confined in the LP_{01} mode with an insertion loss as low as 0.6 dB which includes two S-bend loss at the stress points and two splicing loss between SMF and TMF. At the dips, the light in the LP_{01} mode shows a growing loss with the increase of the applied force, which means that the light is gradually transferred from the LP_{01} to LP_{11} modes and, hence, the conversion efficiency is accordingly increased. Figure 4(b) shows the mode conversion efficiency as the function of the applied force. When the applied force was increased from 0 to 250 g with a mass scale of 25 g, the dip gradually grew to −23 dB, and the conversion efficiency accordingly increased to 99.5%, which is characterized by the pentagram symbols in Fig. 4(b).

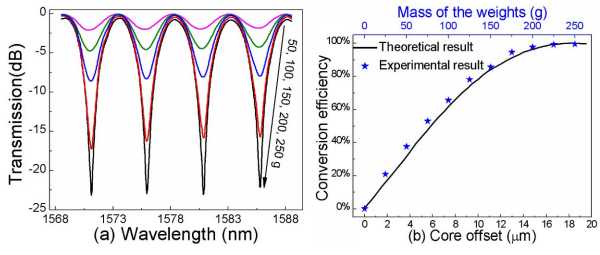

Fig. 4. Influence of the applied force on the mode converter with $L = 75$ cm. The evolution of (a) transmission spectrum and (b) theoretical and experimental mode conversion efficiencies.

On the other hand, we theoretically analyzed the influence of the applied force on the mode conversion efficiency. Since the lateral stress point can be recognized as an S-bend section, the variation of the applied force naturally changes the value of the core-offset at the S-bend section. Therefore, we theoretically calculated the influence of the core-offset on the mode conversion efficiency by substituting the coupling ratio in Fig. 2(b) into Eq. (4). As a result, a theoretical curve was obtained to indicate the mode conversion efficiency as a function of the core-offset from 0 to 19.5 nm with an interval of 0.5 nm. Comparing the theoretical curve with the experimental points, it is found that the measured conversion efficiency majorly agrees with the theoretical predict. Any slight variation between the simulation and experiment can be attributed to the margin of error in the length of S-bend section and measuring the applied force.

We constructed a series of mode converters by increasing the length from 5 to 75 cm with a scale step of 5 cm, and all transmission spectra exhibited comb-like fringe patterns with multiple mode conversion channels. Figure 5(a) illustrates typical transmission spectra of the mode converters with $L = 5$ and 75 cm. The transmission spectra have multi-channels in the C + L band, and the channel spacing is dependent on the length of the mode converter. For instance, when we increased the length from 5 to 75 cm, the channels spacing decreased from 70 to 5 nm, and the channel numbers accordingly increased from 2 to 20. Experimentally, we measured the channel spacing of all mode converters with the length from 5 to 75 cm, and the experimental results were summarized as the sphere symbols in Fig. 5(c). For obtaining the theoretical curve, we first calculated the effective refractive index difference between the LP_{01} and LP_{11} modes by using a numerical mode solver [21,22], and then obtained a differential group effective refractive index around 7.0×10^{-4}, as shown in Fig. 5(b). Finally, we numerically calculated the theoretical channel spacing curve as a function of the fiber length, as shown in Fig. 5(c). It is found that the measured channel spacing almost completely follows the theoretical tendency.

Besides the transmission spectra, we measured the output near-field patterns for directly confirming the mode conversion from the LP_{01} to the LP_{11} mode at the transmission dips. As shown in Fig. 3(b), we used a tunable laser and an infrared camera to inspect the near-field patterns. The tunable laser (TSL210, Santec) has a tuning range of 1500 to 1630 nm. Compared with Fig. 3(a), this experiment removed the second mode stripper on the output side to inject the output mode from the TMF into a microscope objective directly. Figure 6(a) shows the transmission spectrum around a certain

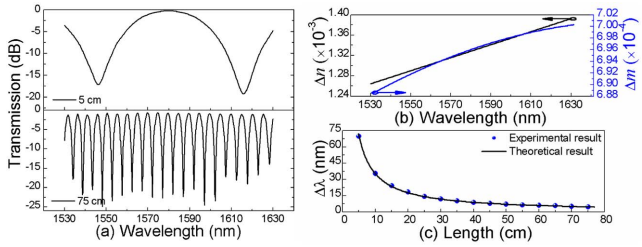

Fig. 5. (a) Transmission spectra of the mode converters with $L = 5$ cm (top panel) and $L = 75$ cm (bottom panel). (b) Calculated mode effective refractive index difference and differential group effective refractive index. (c) Calculated and measured channel spacing as a function of the length of the mode converters.

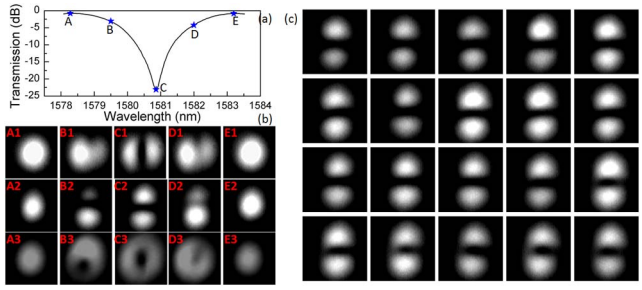

Fig. 6. (a) Transmission spectrum with a single dip at 1580.84 nm. (b) Near-field patterns at the points A, B, C, D, and E in (a). (c) Near-field LP_{11} mode patterns at 20 channel wavelengths. The mode conversion at 20 channels was recorded in Visualization 1.

transmission dip for the 75 cm mode converter. We selected five typical wavelengths to cover different parts of the spectrum, including the dip (Point C, 1580.84 nm), two adjacent peaks (Points A, 1578.28 nm and E, 1583.20 nm), and two middle positions (Points B, 1579.50 nm and D, 1582.00 nm). Figure 6(b) illustrates the captured near-field output patterns at these five wavelengths. Initially, the wavelength of the tunable laser locates at the left peak, and the output pattern shows a pure LP_{01} mode (A1, A2, and A3). As the wavelength gradually moves towards the dip, the output pattern starts to show the contribution from the LP_{11} mode (B1, B2, and B3) and, until the dip, the output pattern shows a pure LP_{11} mode (C1, C2, and C3). When the wavelength moves away from the dip, the LP_{11} mode component gradually diminishes, and the output pattern shows a mixture between the LP_{01} and LP_{11} modes. When the wavelength arrived at the next the peak, the output pattern shows the LP_{01} mode again. The evolution of the mode pattern proves that the LP_{01} mode is completely converted into the LP_{11} mode at the dip in the transmission spectra.

Typically, we can obtain three LP_{11} mode patterns with different shapes by adjusting the polarization state of the input light. In Fig. 6(b), C1 and C2 show the scalar LP_{11} mode patterns with two lobes and orthogonal orientations, called LP_{11a} and LP_{11b}. C3 shows the vector mode pattern with a similar donut shape. Actually, the TMF supported four second-order vector modes, namely, TE_{01}, TM_{01}, HE_{21}^{even}, and HE_{21}^{odd}. Therefore, the transmission dips in Fig. 5(a) are actually generated by converting the LP_{01} mode to any of these vector modes or a mix of them, depending on the polarization state of the LP_{01} mode launched into the converter. By carefully adjusting the polarization state of the input mode, we could separately generate all four vector modes, which showed similar donut-shaped mode patterns. To identify these vector modes, we placed a rotatable polarizer after the microscope objective and analyzed the relationship between the orientations of the polarizer and the orientations of the two lobes in the inspected patterns. Here, we only gave an example of HE_{21}^{odd} mode (C3) in Fig. 6.

Moreover, we measured the near-field mode patterns at all dips in the transmission spectrum [bottom panel in Fig. 5(a)] of the mode converter with $L = 75$ cm. The wavelength of the tunable laser was sequentially switched at the 20 dips in the wavelength range from 1530 to 1630 nm. The state of the input polarization controller was adjusted at the channel wavelength of 1580.84 nm, and then it was maintained throughout all 20 channels. Figure 6(c) illustrates the near-field LP_{11} mode patterns at 20 channels. From these mode patterns, it can be confirmed that the proposed mode converter can realize mode conversion from the LP_{01} to LP_{11} modes at all 20 channels.

In conclusion, we have investigated the multi-channel mode converter via a modal interferometer in the TMF. The interference spectra exhibited multiple dips at which the input LP_{01} mode was converted into the LP_{11} mode. The mode conversion efficiency has been optimized to be 99.5%, and the operation channels reached up to 20. The near-field mode patterns confirmed that such a multi-channel mode conversion in a TMF has been realized efficiently.

Funding. National Natural Science Foundation of China (NSFC) (61405128, 61377066, 61475029, 61520106012, 61635004); Fundamental Research Funds for the Central Universities Key Research and Development (106112017CDJXY120002); Ministry of Science and Technology of the People's Republic of China (MOST) (2016YFC0801200); Science Fund for Distinguished Young Scholars of Chongqing (CSTC2014JCYJJQ40002).

REFERENCES

1. R. J. Essiambre and R. W. Tkach, Proc. IEEE **100**, 1035 (2012).
2. D. J. Richardson, J. M. Fini, and L. E. Nelson, Nat. Photonics **7**, 354 (2013).
3. A. Li, A. Al Amin, X. Chen, and W. Shieh, in *Optical Fiber Communication Conference* (Optical Society of America, 2011), paper PDPB8.
4. T. Mizuno, H. Takara, A. Sano, and Y. Miyamoto, J. Lightwave Technol. **34**, 582 (2016).
5. H. J. Von, R. Ryf, and P. Winzer, Opt. Express **21**, 18097 (2013).
6. W. Q. Thornburg, B. J. Corrado, and X. D. Zhu, Opt. Lett. **19**, 454 (1994).
7. M. Salsi, C. Koebele, D. Sperti, P. Tran, H. Mardoyan, P. Brindel, H. Mardoyan, S. Bigo, A. Boutin, F. Verluise, P. Sillard, M. Astruc, L. Provost, F. Cerou, and G. Charlet, J. Lightwave Technol. **30**, 618 (2012).
8. D. Melati, A. Alippi, and A. Melloni, Opt. Express **24**, 12625 (2016).
9. R. Ismaeel, T. Lee, B. Oduro, Y. Jung, and G. Brambilla, Opt. Express **22**, 11610 (2014).
10. J. D. Love and N. Riesen, Opt. Lett. **37**, 3990 (2012).
11. S. Gross, N. Riesen, J. D. Love, and J. W. Michael, Laser Photon. Rev. **8**, L81 (2014).
12. N. K. Fontaine, R. Ryf, J. Bland-Hawthorn, and S. G. Leon-Saval, Opt. Express **20**, 27123 (2012).
13. M. M. Ali, Y. Jung, K. S. Lim, M. R. Islam, S. U. Alam, D. J. Richardson, and H. Ahmad, IEEE Photon. Technol. Lett. **27**, 1713 (2015).
14. Y. Zhao, Y. Liu, L. Zhang, C. Zhang, J. Wen, and T. Wang, Opt. Express **24**, 6186 (2016).
15. J. Dong and K. S. Chiang, IEEE Photon. Technol. Lett. **27**, 1006 (2015).
16. W. Zhang, L. Huang, K. Wei, P. Li, B. Jiang, D. Mao, F. Gao, T. Mei, G. Zhang, and J. Zhao, Opt. Express **24**, 10376 (2016).
17. R. C. Youngquist, J. L. Brooks, and H. J. Shaw, Opt. Lett. **9**, 177 (1984).
18. S. Ramachandran, P. Kristensen, and M. F. Yan, Opt. Lett. **34**, 2525 (2009).
19. I. Giles, A. Obeysekara, R. Chen, D. Giles, F. Poletti, and D. Richardson, IEEE Photon. Technol. Lett. **24**, 1922 (2011).
20. A. Li, A. Amin, X. Chen, S. Chen, G. Gao, and W. Shieh, J. Lightwave Technol. **30**, 634 (2012).
21. G. Yin, S. Lou, Q. Li, and H. Zou, Opt. Laser Technol. **48**, 60 (2013).
22. Y. C. Lu, L. Yang, W. P. Huang, and S. S. Jian, J. Lightwave Technol. **26**, 1868 (2008).